Electron-spin-resonance study of Pb_2^{3+} dimer centers in NaCl:$PbCl_2$

I. Heynderickx, E. Goovaerts, and D. Schoemaker
Physics Department, University of Antwerp (Universitaire Instelling Antwerpen), B-2610 Wilrijk-Antwerpen, Belgium
(Received 8 December 1986)

A quantitative analysis is presented for the electron-spin-resonance spectra of five new defects, which are produced in NaCl:$PbCl_2$ samples by an x irradiation at 77 K and eventual thermal anneal to higher temperatures. The symmetry which is near to orthorhombic along, e.g., ([100],[001],[1$\bar{1}$0]) axes, and the resolved hyperfine structure lead for all these defects to a model consisting essentially of a trapped electron Pb_2^{3+} lead dimer center. A quantitative analysis is performed on the g components and the hyperfine interaction in terms of the molecular structure. The absence of Pb_2^{3+} defects in KCl:$PbCl_2$ samples indirectly demonstrates the different aggregation behavior of divalent impurity-cation vacancy dipoles in both hosts.

I. INTRODUCTION

Spectroscopic techniques such as optical absorption, luminescence excitation transfer, Raman scattering, ionic thermocurrent, and electron spin resonance (ESR) are widely used to monitor the aggregation and precipitation of divalent ion-cation vacancy (IV) dipoles in alkali halides.[1] Many of these studies have been performed on crystals doped with the paramagnetic Mn^{2+} (Refs. 2–4) and the diamagnetic Pb^{2+} (Refs. 5–8) ions. The aggregation of impurities which are not optically visible, such as Ca^{2+}, Sr^{2+}, and Cd^{2+}, is often investigated by incorporating Pb^{2+} ions as a second impurity in the crystals.[1] Those spectroscopic results lead to a detailed description of two possible clustering mechanisms:[9] either aggregation from trimers to pentamers, heptamers, etc. by adding each time one dimer, or precipitation to a Suzuki phase, the structure of which can be observed in x-ray diffraction.[10]

Some years ago a comparative study on lead-doped KCl and NaCl crystals was undertaken[5,6,11] in order to determine the kind of clustering in these samples. In the former, clusters consisting of trimers, pentamers, etc. are produced during the first stages of the aggregation mechanism and finally $PbCl_2$ precipitates are formed. In the latter only Suzuki phase precipitates develop after high-temperature (above 440 K) aging experiments. Moreover, it is demonstrated that the aggregation in NaCl proceeds considerably faster than in KCl. In the present paper this behavior is indirectly confirmed by comparing the results of an ESR study on NaCl:$PbCl_2$ crystals with those of KCl:$PbCl_2$ and RbCl:$PbCl_2$ crystals, discussed earlier.[12,13]

When either a quenched KCl:$PbCl_2$ or RbCl:$PbCl_2$ crystal is x-irradiated at liquid-nitrogen temperature (LNT) or room temperature (RT), several paramagnetic defects are observed, which each essentially consist of a hole or one or several electrons trapped at an isolated Pb^{2+}-cation vacancy dipole. ESR studies on lead-doped KCl samples have revealed the characteristic structure of the trapped hole Pb^{3+} defect[14] and the trapped electron $Pb^+(Cl_i^-)$ (Ref. 12), Pb^- (Ref. 15) and $Pb^+(1)$ defects.[13] The existence of the so-called primary trapped electron $Pb^+(0)$ center[16] has only been demonstrated in optical-absorption measurements. On the other hand, in lead-doped RbCl samples the $Pb^+(Cl_i^-)$ defect[12] and the so-called $Pb^+(1)$ defects[13] were studied together with their counterparts in KCl, but until now no results have been reported about the $Pb^+(0)$, Pb^-, or Pb^{3+} defects.

Optical absorption of the primary trapped electron $Pb^+(0)$ center has also been observed in quenched and x-irradiated NaCl:$PbCl_2$ crystals.[16] Our ESR results on such samples, however, mainly show the presence of defects consisting essentially of an electron trapped by a dimer of Pb^{2+} ions. Consequently, these centers will be called "Pb_2^{3+} centers." Similar dimer defects have been studied in heavily doped KCl:TCl crystals, namely, the so-called $Tl_2^+\langle 110\rangle$ (Ref. 17) and $Tl_2^+\langle 111\rangle$ (Ref. 18) centers. The former, produced by a short x irradiation at 77 K, consists of an electron, trapped by two adjacent substitutional Tl^+ ions and as a result, the molecule is directed along a $\langle 110\rangle$ axis. The proposed model for the latter, which is quite easily produced by an x-irradiation at temperatures above 220 K, consists of a Tl_2^+ molecule ion on a single cation site which is oriented along a $\langle 111\rangle$ direction.

In Sec. II we present the analysis of the ESR spectra of the Pb_2^{3+} centers in NaCl:$PbCl_2$ crystals. The influence of the presence of oxygen impurities on the detailed defect structure is checked by comparing the spectra of NaCl crystals, to which 0.1 mol % $PbCl_2$ was added in the melt and which were grown by the Kyropoulos method in air, to those of NaCl crystals, to which 0.2 mol % $PbCl_2$ was added and which were grown by the Bridgman-Stockbarger method in a reactive atmosphere. The hyperfine (hf) interaction of the paramagnetic electron with the ^{207}Pb nuclei was measured in an oxygen-free NaCl crystal, which was grown from a melt containing 0.13 mol % of the 92% enriched $^{207}PbCl_2$. Section III contains some typical production properties of the Pb_2^{3+} defects. In Sec. IV we discuss the proposed model for the essential core of the structure of those defects.

II. QUANTITATIVE ANALYSIS

A. Determination of the g tensor

X irradiation of a quenched NaCl:$PbCl_2$ sample at LNT and a subsequent pulse anneal to a temperature between LNT and RT generates, apart from the spectrum of the V_K center[19] and the Pb^{3+} defect, a number of resonance lines which are attributed to Pb-associated defects (Figs. 1 and 2). The spectra are all recorded at 15 K and at a microwave power of 100 mW. The angular dependence of the resonance spectra observed for a rotation of the static magnetic field **H** in a (100) plane of the crystal shows a symmetry close to orthorhombic along a set of (x,y,z) axes being, e.g., ([110],[001],[1$\bar{1}$0]). We will designate the resonance lines by their polar angles θ and ϕ, describing the orientation of **H** with respect to these (x,y,z) axes.

According to the natural abundance of 79% for the ^{even}Pb isotopes without nuclear spin ($I=0$), the dominant contribution to the ESR lines of a NaCl:$PbCl_2$ crystal originates from paramagnetic electrons interacting with ^{even}Pb nuclei. Consequently, for such species the principal values of the g tensor along the (x,y,z) axes are obtained by describing the resonance lines in terms of a spin Hamiltonian, containing only the Zeeman interaction for a value of the electron spin $S=\frac{1}{2}$ (usual notation):

$$\frac{\mathcal{H}}{g_0\mu_B}=\frac{1}{g_0}\mathbf{H}\cdot\bar{g}\cdot\mathbf{S}\ . \tag{1}$$

The g parameters, resulting from an analysis of the spectra (Figs. 1 and 2) measured after a specific thermal an-

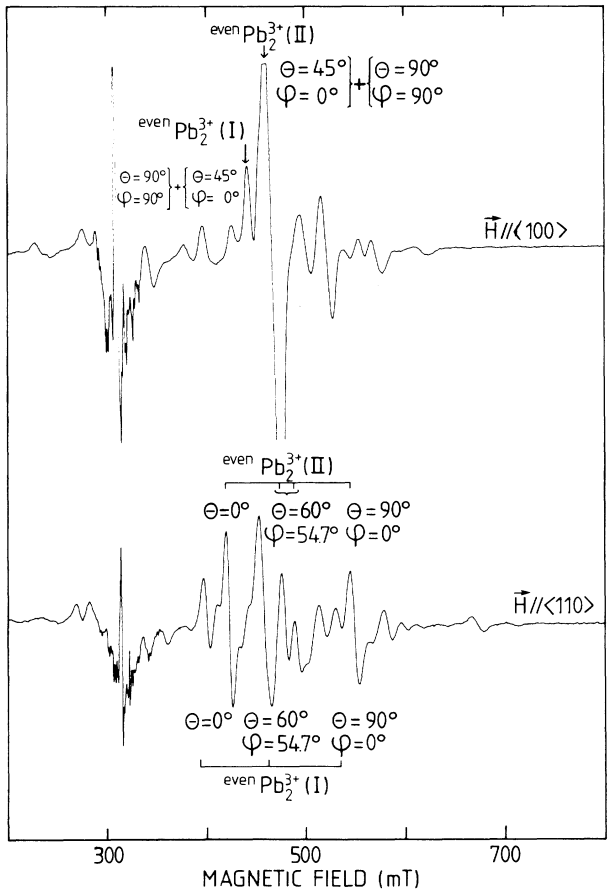

FIG. 1. The ESR spectra of the Pb_2^{3+}(I) and Pb_2^{3+}(II) defects in a NaCl:$PbCl_2$ sample, which is x-irradiated for 90 min at LNT. The X-band spectra ($\nu=9.28$ GHz) are recorded at 15 K for an external magnetic field along the ⟨100⟩ and ⟨110⟩ crystallographic axes.

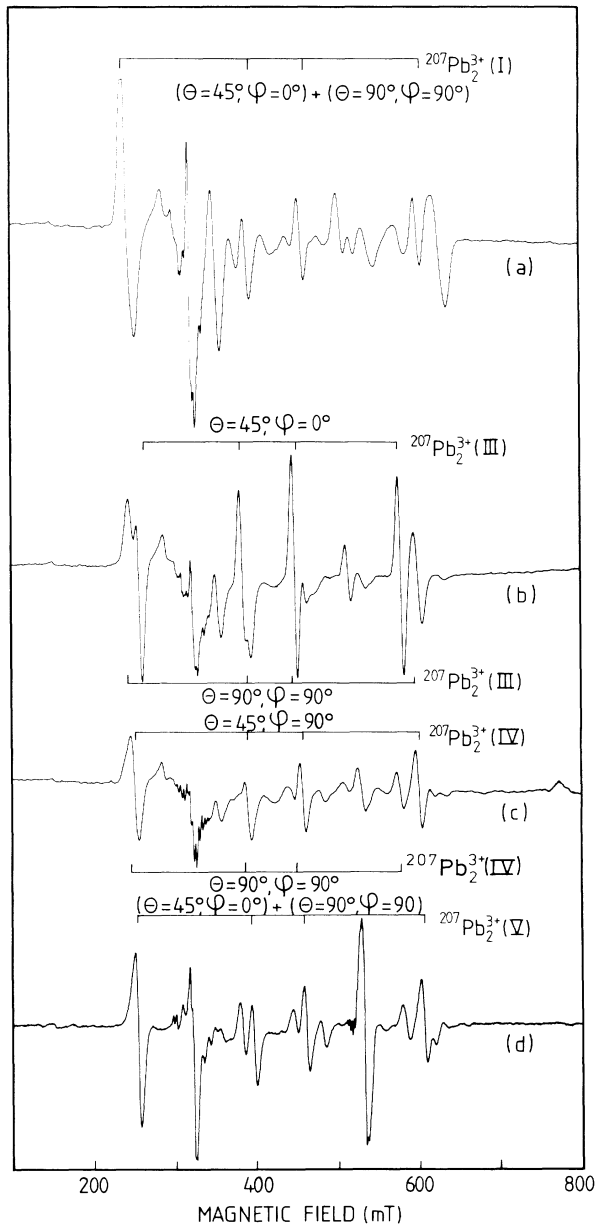

FIG. 2. The X-band ESR spectra ($\nu=9.28$ GHz) for an external magnetic field along a ⟨100⟩ direction are recorded at 15 K in a NaCl:$^{207}PbCl_2$ crystal after 120 min of x irradiation at LNT (a), and a subsequent thermal anneal to appropriate temperatures: (b) to 150 K; (c) to 240 K; and (d) to RT.

nealing treatment (Sec. III) are given in Table I. There, the different centers are enumerated in parentheses by a roman numeral.

Characteristic for all these centers is the large anisotropy in the (x,y) plane: the g_y is almost equal to the mean value of g_x and g_z. In Fig. 3 the angular dependence for rotation in a (100) plane is shown for the Pb_2^{3+}(III) defect, described by g values which exactly obey the relation $g_y^2=\frac{1}{2}(g_x^2+g_z^2)$. This modifies the picture for an angular variation in a (100) plane in the case of orthorhombic symmetry along $\langle 110\rangle$ axes so that the $(\theta=45°, \phi=0°)$ resonance line becomes accidentally degenerate with the $(\theta=90°, \phi=90°)$ line.

For three Pb_2^{3+} defects the z axis of the g tensor is tilted away from the $[1\bar{1}0]$ axis in the (110) plane over an angle γ, given in Table I. The presence of such a tilting is demonstrated by a shift of the $(\theta=90°, \phi=90°)$ resonance line and a splitting of the $(\theta=60°, \phi=54.7°)$ resonance line. The latter is illustrated in Fig. 1 for the Pb_2^{3+}(II) center and in Fig. 4 for the Pb_2^{3+}(IV) defect. These effects were not observed for the remaining defects mentioned in Table I, and because of the experimental linewidth of about 8 mT for the resonance lines we can conclude that if a tipping angle is present, it will be smaller than 2.5°.

B. Determination of the hyperfine tensor

In the ESR spectra or NaCl crystals, enriched with the $^{207}Pb^{2+}$ isotope with nuclear spin $I=\frac{1}{2}$, one observes for each of the defects a splitting of the $I=0$ resonance line into four lines of nearly equal intensity (Fig. 2). Such a hyperfine structure is characteristic for the interaction of an $S=\frac{1}{2}$ electron spin with two $I_i=\frac{1}{2}$ nuclear spins. One of the lines, however, is situated within the experimentally measured linewidth at the same magnetic field position as the analyzed $I=0$ line (Sec. II A). This is only possible in the case of two nearly equivalent $I_i=\frac{1}{2}$ nuclei, for which the nuclear spins $\mathbf{I}_i$ combine in a good approximation to a total nuclear spin $\mathbf{I}$ ($I=0,1$). The splitting into *four* lines is now explained by the assumption of hf terms which are sufficiently large compared to the Zeeman energy.

The principal values of the A tensor, which describes this interaction, are obtained by fitting the experimental data to the spectra predicted by the spin Hamiltonian

TABLE I. The principal values of the g tensor and the tipping angle, γ, of the z axis away from $[1\bar{1}0]$ in a (110) plane, are given for the Pb_2^{3+} centers in NaCl:$PbCl_2$. The accuracy is approximately 0.002 on the g values and 0.5° on the tipping angle.

Defect	g_x [110]	g_y [001]	g_z $[1\bar{1}0]$	γ (deg)
Pb_2^{3+}(I)	1.222	1.438	1.625	0
Pb_2^{3+}(II)	1.188	1.479	1.537	6.7
Pb_2^{3+}(III)	1.300	1.469	1.621	0
Pb_2^{3+}(IV)	1.231	1.462	1.638	16.4
Pb_2^{3+}(V)	1.237	1.428	1.597	4.2

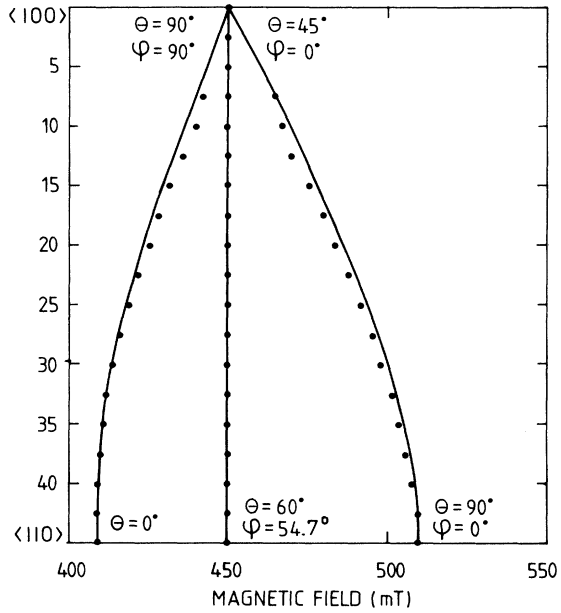

FIG. 3. The angular variation of the ESR spectra for the $^{even}Pb_2^{3+}$(III) defect in NaCl:$PbCl_2$ is given for a rotation of the external magnetic field $\mathbf{H}$ in a (100) plane of the crystal. The experimental results, represented by the dots, are compared with the solid lines, showing the theoretically calculated angular dependence.

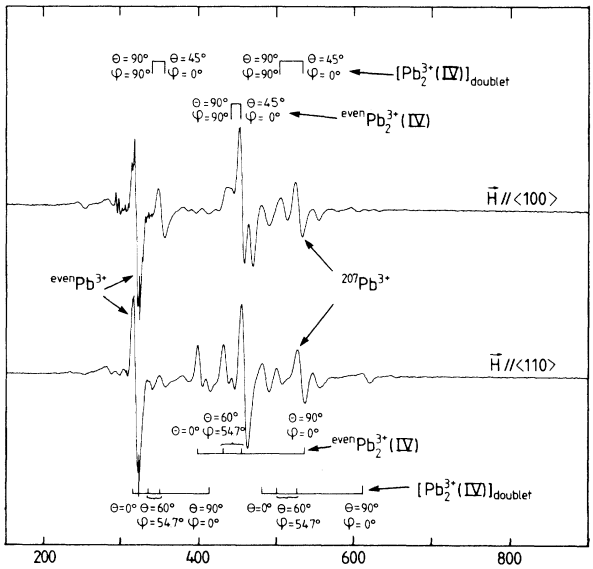

FIG. 4. The ESR lines ($\nu=9.28$ GHz) of the Pb_2^{3+}(IV) defect in NaCl doped with Pb^{2+} according to its natural isotope abundance, are shown for an external magnetic field $\mathbf{H}$ along $\langle 100\rangle$ and $\langle 110\rangle$ crystallographic axes ($T=15$ K). The lines denoted by $^{even}Pb_2^{3+}$(IV) involve two ^{even}Pb nuclei, while those denoted by $[Pb_2^{3+}(IV)]_{doublet}$ involve one ^{even}Pb and one ^{207}Pb nucleus.

(usual notation):

$$\frac{\mathcal{H}}{g_0\mu_B}=\frac{1}{g_0}\mathbf{H}\cdot\bar{g}\cdot\mathbf{S}+\mathbf{S}\cdot\bar{A}\cdot\mathbf{I}\ , \tag{2}$$

with $S=\frac{1}{2}$ and $I=0,1$, and in which the g values of Table I are substituted. This fitting is performed with the so-called "simulated-anneal" method,[20] which is a recently developed minimization procedure based on the Metropolis Monte Carlo algorithm. The results of this analysis, in which it is assumed that the principal axes of the A tensor coincide with the principal axes of the g tensor, are given for the Pb_2^{3+}(I), Pb_2^{3+}(III), Pb_2^{3+}(IV), and Pb_2^{3+}(V) centers in Table II. In contrast to the large anisotropy in the g values, the A parameters are nearly isotropic. Consequently, the hf lines exhibit qualitatively the same angular dependence of the magnetic field for rotation in a (100) plane as the $I=0$ resonance lines.

For a NaCl crystal, doped with Pb^{2+} ions according to their natural abundance of isotopes, i.e., 79% of the ^{even}Pb nuclei with $I_i=0$ and 21% of the ^{207}Pb nuclei with $I_i=\frac{1}{2}$, one can determine the expected intensity for each of the possible combinations of the isotopes in the Pb_2^{3+} dimer. The ^{even}Pb-^{even}Pb combination occurs for 62% and causes no splitting of the resonance lines. The ^{even}Pb-^{207}Pb combination has an abundance of 34% and because of its doublet structure each of the resonance lines will reach an intensity of 17%. The ^{207}Pb-^{207}Pb combination occurs for only 4% and because of the corresponding quartet structure the lines will have a negligible intensity of 1%. For the Pb_2^{3+}(IV) defect the doublet structure of the electron interacting with a ^{207}Pb nucleus and a ^{even}Pb nucleus is shown in Fig. 4.

For the Pb_2^{3+}(II) defect the resonance lines in our NaCl:$^{207}PbCl_2$ samples were absent for an unknown reason. In principle, however, the A values can now be determined from the doublet structure, which is detected in NaCl:$PbCl_2$ samples, doped with Pb^{2+} ions according to their natural abundance. Because of the simultaneous occurrence of the Pb_2^{3+}(I) defect with the Pb_2^{3+}(II) defect, a sufficiently accurate identification of the resonance lines, and as a consequence an analysis of the hf interaction, was made impossible for the latter defect.

TABLE II. The hyperfine components, the anisotropic part ρ_s, and isotropic part A_σ of the hyperfine interaction are given in units of mT for the Pb_2^{3+} centers in NaCl:$^{207}PbCl_2$. Signs of the hyperfine components are attributed according to the constraint of a positive and constant ρ_s value. Errors are estimated to be 1 mT.

Defect	A_x [110]	A_y [001]	A_z [1$\bar{1}$0]	ρ_s	A_σ
Pb_2^{3+}(I)	−117	−122	+125	+47	−17
Pb_2^{3+}(III)	−115	−123	+115	+48	−23
Pb_2^{3+}(IV)	−121	−120	+123	+48	−18
Pb_2^{3+}(V)	−114	−121	+126	+48	−17

C. Discussion of the g tensor

Since the Pb_2^{3+} dimer center consists of a single valence electron trapped by two $6s^2$ Pb^{2+} ions, its electronic configuration is equal to the one of the Tl_2^+ centers[17,18] and complementary to that of the V_K center.[19] The molecular σ_g ground orbital, which is considered as a linear combination of the atomic orbitals, namely

$$\sigma_g=\alpha_g(6s_1+6s_2)+\beta_g(6p_{z,1}-6p_{z,2})\ ,$$

is singly occupied. The excited $\pi_g^x=\mu_g(6p_{x,1}-6p_{x,2})$ and $\pi_g^y=\mu_g(6p_{y,1}-6p_{y,2})$ orbitals, separated from the ground state by an energy E_{1g} and E_{2g}, respectively, are mixed into σ_g by spin-orbit interaction. Their energy values can be determined from the experimentally measured g shifts by a perturbation calculation, pushed to second order with spin-orbit coupling as perturbation.[19] The complete expressions for a Pb_2^{3+} center in an orthorhombic crystal field are given by

$$\Delta g_z=g_0-g_z=ab\lambda_g^2\left[\frac{1}{E_{1g}^2}-\frac{1}{E_{2g}^2}\right]\delta_z-2a^2b^2\lambda_g^2\left[\frac{1}{E_{1g}^2}+\frac{1}{E_{2g}^2}\right]\delta_z-(a^2-b^2)^2\frac{\lambda_g^2}{E_{1g}E_{2g}}\delta_z$$
$$+\lambda_g^2\left[\frac{1}{E_{1g}^2}+\frac{1}{E_{2g}^2}\right]+2ab\lambda_g^2\left[\frac{1}{E_{2g}^2}-\frac{1}{E_{1g}^2}\right]\ , \tag{3a}$$

$$\Delta g_x=g_0-g_x=-2\frac{ab\lambda_{g,y}}{E_{1g}}\delta_x+2\frac{a^2\lambda_{g,x}}{E_{1g}}\delta_x+2\frac{ab\lambda_{g,y}}{E_{2g}}\delta_x+2\frac{b^2\lambda_{g,x}}{E_{2g}}\delta_x+2\frac{a^2b^2\lambda_g'\lambda_g}{E_{1g}^2}\delta_x+2\frac{a^2b^2\lambda_g'\lambda_g}{E_{2g}^2}\delta_x$$
$$-2\frac{a^2ab\lambda_g'\lambda_g}{E_{1g}^2}\delta_x+2\frac{b^2ab\lambda_g'\lambda_g}{E_{2g}^2}\delta_x+\frac{(b^2-a^2)\lambda_g'\lambda_g}{E_{1g}E_{2g}}(b^2-a^2-2ab)\delta_x$$
$$+\tfrac{1}{2}\lambda_g^2\left[\frac{1}{E_{1g}^2}+\frac{1}{E_{2g}^2}\right]+ab\lambda_g^2\left[\frac{1}{E_{2g}^2}-\frac{1}{E_{1g}^2}\right]\ , \tag{3b}$$

$$\Delta g_y = g_0 - g_y = -2\frac{ab\lambda_{g,x}}{E_{1g}}\delta_y + 2\frac{b^2\lambda_{g,y}}{E_{1g}}\delta_y + 2\frac{ab\lambda_{g,x}}{E_{2g}}\delta_y + 2\frac{a^2\lambda_{g,y}}{E_{2g}}\delta_y + 2\frac{a^2b^2\lambda_g'\lambda_g}{E_{1g}^2}\delta_y + 2\frac{a^2b^2\lambda_g'\lambda_g}{E_{2g}^2}\delta_y$$
$$-2\frac{b^2ab\lambda_g'\lambda_g}{E_{1g}^2}\delta_y + 2\frac{a^2ab\lambda_g'\lambda_g}{E_{2g}^2}\delta_y + \frac{(a^2-b^2)\lambda_g'\lambda_g}{E_{1g}E_{2g}}(a^2-b^2-2ab)\delta_y$$
$$+\tfrac{1}{2}\lambda_g^2\left[\frac{1}{E_{1g}^2}+\frac{1}{E_{2g}^2}\right]+ab\lambda_g^2\left[\frac{1}{E_{2g}^2}-\frac{1}{E_{1g}^2}\right]. \tag{3c}$$

In the second-order terms of these expressions the approximation $\lambda_{g,x}=\lambda_{g,y}=\lambda_g$ is introduced, in which $\lambda_{g,x}$ and $\lambda_{g,y}$ are the matrix elements of the x and y component, respectively, of the orbital part of the spin-orbit coupling between the ground state and the excited states. The resulting λ_g and also the parameter λ_g', which yields the expectation value of the z component of the orbital part of the spin-orbit coupling between the π_g, are given as a function of the molecular-orbital coefficients μ_g and β_g, and of the atomic spin-orbit–coupling constant $\lambda>0$ by the relations

$$\lambda_g = 2\mu_g\beta_g\lambda\ , \tag{4a}$$

$$\lambda_g' = 2\mu_g^2\lambda\ . \tag{4b}$$

The numerical values for μ_g and β_g are taken from Ref. 19. In order to reduce the number of unknown parameters in Eq. (3), the approximation $\lambda_{g,x}=\lambda_{g,y}$ is also extended to the first-order terms. In analogy to Ref. 17 we will approximate the δ_i $(i=x,y,z)$ values, which are the matrix elements of the corresponding component of the orbital-momentum operator in the Zeeman interaction, by the relation $\delta_x=\delta_y=\delta$ and $\delta_z=0.8$. The latter approximation was discussed in Ref. 17 and used here in order to have the possibility of comparing the results. The coefficients a and b in the excited states are given by

$$a = k_g\lambda_g' \tag{5a}$$

$$b = k_g[\Delta_g - (\Delta_g^2+\lambda_g'^2)^{1/2}]\ , \tag{5b}$$

in which k_g is the normalization constant such that $a^2+b^2=1$. The crystal-field contribution Δ_g can be expressed in terms of the energy difference by the zeroth-order relation:

$$E_{2g}-E_{1g} = (\Delta_g^2+\lambda_g'^2)^{1/2}\ . \tag{6}$$

For the $Tl_2^+\langle 110\rangle$ and Pb_2^{3+} defects the higher-order terms to (6) give a correction of less than 10%.

We want to remark that the expression (2) of Ref. 17 and (11) of Ref. 19 are incomplete as a consequence of an inconsistent approximation. But this does not influence the final results, since the axial approximation to the set of equations (3) yields the same expressions as those derived from the incomplete formulas of Refs. 17 and 19. In contrast to Ref. 17, however, the axial approximation in the description of the electronic structure is not applied here because of the large anisotropy between the g_x and g_y for all the Pb_2^{3+} defects. Consequently, a system of four nonlinear equations, of which three are given by the g-shift expressions (3) and the fourth by the normalization condition, has to be solved in terms of the parameters E_{1g}, E_{2g}, δ, and k_g. The influence of the axial approximation is investigated by comparing the solution of this problem for the $Tl_2^+\langle 110\rangle$ center[17] and the Pb_2^{3+}(III) center to the parameters E_{1g}, E_{2g}, δ, and k_g obtained from the calculation procedure of Ref. 17 for $\delta_z=0.8$. The data are listed in Table III.

It seems that for each of the defects the orthorhombic approach increases the values of δ and lowers the excitation energies. As a result the orthorhombic description nearly reproduces the δ value for the $Tl_2^+\langle 110\rangle$ center, which in Ref. 17 was theoretically estimated to be 0.67. The δ value of the Pb_2^{3+}(III) defect, however, is unreasonably small even in the orthorhombic approach.

TABLE III. Comparison of δ, the normalization constant k_g, and the excitation energies E_{1g} and E_{2g} in an axial approximation and in an orthorhombic description of the electronic structure for the $Tl_2^+\langle 110\rangle$ defect in KCl and the Pb_2^{3+}(III) defect in NaCl.

Defect	E_{1g} (eV)	E_{2g} (eV)	$\delta\equiv -i\langle\sigma_g \mid l_x \mid \pi_g\rangle$	k_g (eV^{-1})
$Tl_2^+\langle 110\rangle$[a]	0.95	1.75	0.52	1.20
Axial	±0.05	±0.05	±0.03	±0.05
$Tl_2^+\langle 110\rangle$[a]	0.75	1.58	0.60	1.23
Orthorhombic	±0.01	±0.01	±0.01	±0.01
Pb_2^{3+}(III)	1.00	2.95	0.20	0.70
Axial	±0.05	±0.05	±0.03	±0.05
Pb_2^{3+}(III)	1.07	2.75	0.30	0.69
Orthorhombic	±0.02	±0.02	±0.02	±0.02

[a]Reference 17.

This can be seen from the approximate expression which allows an estimate of the interatomic distance R:[17]

$$R=\frac{1-\delta}{\alpha_g\mu_g\langle 6x \mid \partial/\partial x \mid 6p_x\rangle} . \tag{7}$$

Additional inaccuracy is introduced in this expression by the substitution of the approximate values of Ref. 19 for α_g, μ_g, and the gradient integral, the numerical value of which is unknown for a Pb_2^{3+} molecule. It results in a distance of 15 a.u., which we believe is much too large, mainly because of the small value of δ.

For the excitation energies of the $Tl_2^+\langle 110\rangle$ center a small discrepancy is found between the calculated energies and the detected optical-absorption bands, which are situated at 0.70 and 1.44 eV. However, we have to keep in mind that the $\sigma_g\rightarrow\pi_g$ transitions are calculated, while optically the $\sigma_g\rightarrow\pi_u$ transitions can be measured. For the Pb_2^{3+} defects, on the other hand, the positions of the absorption bands are still unknown and nothing can be concluded about the reliability of the high values of E_{1g} and E_{2g}. Consequently, it would be worthwhile to determine these positions, e.g., by the optically detected magnetic resonance (ODMR) technique, which allows one to directly connect the absorption bands to the ESR signals.

Finally, we want to mention that a low accuracy was to be expected from this perturbative analysis because of the large spin-orbit–coupling constant: about a factor of 2 larger for the free Pb^+ ion ($\lambda\simeq 9400\ cm^{-1}$) than for the free Tl^0 atom ($\lambda\simeq 5100\ cm^{-1}$). Apart from the errors resulting from the application of the numerical values of Ref. 19 for some of the parameters, additional inaccuracy is introduced by describing the electronic structure of the Pb_2^{3+} defects on the basis of a one-electron, nonrelativistic, second-order perturbation calculation. Those deficiencies will be more important for heavy ions or atoms, possessing a high electron density at the nucleus and a large spin-orbit–coupling constant.

D. Discussion of the hyperfine tensor

The hf components for a diatomic molecule with a single valence electron in p_σ orbitals, characterized by a spin-orbit coupling λ, in an axial approximation for the crystal field with energy E, are given up to second order in λ/E in terms of the g shifts,

$$\Delta g_\parallel=g_0-g_\parallel=\frac{\lambda^2}{E^2} , \tag{8a}$$

$$\Delta g_\perp=g_0-g_\perp=2\frac{\lambda}{E}+2\frac{\lambda^2}{E^2} , \tag{8b}$$

by the expression (for an extended discussion see Refs. 17 and 19)

$$A_\parallel=(1-\tfrac{1}{2}\Delta g_\parallel)A_\sigma+(2+\tfrac{3}{2}\Delta g_\perp-2\Delta g_\parallel)\rho_s+\tfrac{5}{2}\Delta g_\parallel\rho_l , \tag{9a}$$

$$A_\perp=(1-\tfrac{1}{2}\Delta g_\parallel)A_\sigma-(1+\tfrac{3}{4}\Delta g_\perp+\tfrac{1}{4}\Delta g_\parallel)\rho_s -(\tfrac{5}{2}\Delta g_\perp-\tfrac{5}{2}\Delta g_\parallel)\rho_l , \tag{9b}$$

in which $A_\sigma=A_\sigma^e+A_\sigma^s$ is the isotropic part, containing

$$A_\sigma^e=\frac{\mu_I}{I}\beta_g^2\langle r^{-3}\rangle_e ,$$

the exchange polarization contribution;

$$A_\sigma^s=\frac{8\pi}{3}\frac{\mu_I}{I}\alpha_g^2\mid\psi_s(0)\mid^2 ,$$

the Fermi contact term;

$$\rho_s=\frac{2}{5}\frac{\mu_I}{I}\beta_g^2\langle r^{-3}\rangle_s ,$$

the anisotropic part, describing the dipole-dipole interaction between the magnetic moments of the electron and nuclei; and

$$\rho_l=\frac{2}{5}\frac{\mu_I}{I}\beta_g^2\langle r^{-3}\rangle_l ,$$

the anisotropic part, resulting from the interaction between the orbital moments of the electron and the nuclear moments. For many of the atomic and molecular systems it has been found that $\rho_s\simeq 1.13\rho_l$ (Ref. 19).

In order to express the hf components as a function of the g shifts, we have introduced the approximation of axial symmetry. In the case of the Pb_2^{3+} centers, this is a crude approximation, which is, however, necessary because of the complexity of the relations to be applied for orthorhombic symmetry. Since $\Delta g_\parallel$ and $\Delta g_\perp$ are known experimentally, one can calculate the values ρ_s and A_σ of the hf interaction from the determination of the components $A_\parallel$ and $A_\perp$. But in order to do so one needs the signs of $A_\parallel$ and $A_\perp$, which cannot be obtained from the ESR spectra.[21] They are assigned according to the imposed constraint of a constant ρ_s value for the different Pb_2^{3+} defects, possessing the same sign as that of the magnetic moment of the Pb nucleus. For each of the defects the ρ_s and A_σ value are included in Table II.

The calculation procedure in Ref. 17 illustrates that one can estimate the influence of surroundings and molecular structure on the hf interaction by comparing the experimentally determined ρ_s and A_σ values with those obtained from a Hartree-Fock calculation of the $6p$ function of a free Pb^+ ion. Indeed, the ratio of the anisotropic hf term, ρ_s, of a given defect to that of the corresponding free atom or ion gives a measure of the delocalization of the ground orbital of the defect towards the surrounding lattice ions. And, the amount of s mixing into the ground orbital is determined from the difference of the experimentally measured A_σ value with that calculated for the free atom or ion, which contains exclusively the contribution of the exchange polarization, A_σ^e. In this calculation,[17] however, the nonrelativistic limit is substituted in relativistic equations for the hf components. By doing so, errors are introduced, which become large for heavy atoms or ions possessing a high electron density at the nucleus. In particular when the calculation procedure is repeated for lead-associated defects, the results become unreasonable because of the importance of the neglected relativistic and correlation effects. Therefore we have attempted to get an idea of the delocalization and the s mixing by directly comparing the ρ_s and A_σ values of the different Pb^+ defects, namely the $Pb^+(Cl_i^-)$ defect in KCl, the $Pb^+(1)$

defect in KCl, and the Pb_2^{3+}(III) center in NaCl. The corresponding values are given in Table IV.

In our notation β_g^2 determines for a given Pb^+ defect the $6p$ electron density around the nucleus of the Pb^+ ion, while the remaining density is distributed over the ligand ions. For a Pb_2^{3+} defect the molecular wave function of the valence electron is spread over two Pb^{2+} ions. Taking into account the overlap contribution S_{pp} of the atomic $6p$ orbitals in the molecular orbital, its electron density at the nucleus is proportional to $2\beta_g^2(1-S_{pp})$. The value of S_{pp} is positive for a σ_g ground orbital and estimated to be about 0.20. Consequently, one expects for the ratio of the ρ_s values, i.e., the ratio of the β_g^2 values,

$$\frac{\beta_g^2[Pb_2^{3+}]}{\beta_g^2[Pb^+]}=[2(1-S_{pp})]^{-1}=0.63 .$$

This value is surprisingly, but maybe fortuitously, well reproduced by the ratio of the experimentally determined ρ_s values:

$$\frac{\rho_s[Pb_2^{3+}]}{\rho_s[Pb^+]}=0.63 .$$

The A_σ^s value can now be determined from the experimentally measured A_σ value on condition that the contribution of the exchange polarization, A_σ^e, is known. The latter is estimated from the A_σ value of the $Pb^+(Cl_i^-)$ defect, for which the surrounding crystal field is believed to be essentially even and, consequently, little or no A_σ^s contribution is mixed into A_σ.[22] So if we assume that no delocalization occurs for the Pb^+ defects, we find

$$\frac{\mu_I}{I}\langle r^{-3}\rangle_e=-97 \text{ mT} .$$

The A_σ^s value is now given as $A_\sigma-\beta_g^2(\mu_I/I)\langle r^{-3}\rangle_e$ and results in $A_\sigma^s=+40$ mT for the $Pb^{+(1,a)}$ defect in KCl, and $A_\sigma^s=+37$ mT for the Pb_2^{3+}(III) defect in NaCl. The values of the other $Pb^+(1)$ and Pb_2^{3+} defects are slightly different, reflecting the influence of the different crystalline environments. It demonstrates that for both kinds of defects s mixing influences the isotropic part of the hyperfine interaction. For the $Pb^+(1)$ defects it originates from the odd component of the surrounding crystal field due to the presence of an anion vacancy along the [001] crystallographic axis. For the Pb_2^{3+} center it results from the molecular bond.

TABLE IV. The anisotropic part, ρ_s, and the isotropic part, A_σ, of the hyperfine interaction are compared for some Pb-associated defects (in units of mT). The estimated accuracy is 1 mT.

Defect	ρ_s	A_σ
$Pb^+(Cl_i^-)$ in KCl[a]	+76	−97
$Pb^+(1,a)$ in KCl[b]	+74	−57
Pb_2^{3+}(III) in NaCl	+48	−23

[a]Reference 13.
[b]Reference 15.

III. PRODUCTION PROPERTIES

A. Influence of quenching on the production

As mentioned in the Introduction, IV dipoles in alkali halides tend to form aggregates and precipitates. These clusters can however be dissolved in the lattice by heating the crystals to temperatures near the melting point. The dissolved dipoles will be frozen in by quenching the samples as fast as possible to low temperatures, e.g., LNT. The NaCl:$PbCl_2$ crystals were handled in this way before the production of the Pb_2^{3+} dimer centers by x irradiation. The influence of the annealing temperature and the rate of the quenching on the intensity of the ESR lines was studied for equal doses of x irradiation at LNT.

No difference in the concentration of the Pb_2^{3+} centers is observed for samples which are annealed to temperatures between 770 and 920 K, on the condition that they are quenched at the same rate. An intensity decrease of about a factor of 2, however, results from cooling an annealed sample down to LNT within 20 min instead of within 2 min. Moreover, x-irradiating for 1 h a sample that was kept at RT for several months does not produce a detectable concentration of Pb_2^{3+} centers. This suggests that they are produced from a dimer of IV dipoles, occurring during the first stage of the aggregation mechanism in NaCl:$PbCl_2$ crystals.

B. Production by x irradiation at LNT as a function of time

The intensity of the Pb_2^{3+}(II) defect in a quenched NaCl:$PbCl_2$ sample is given in Fig. 5 as a function of the time of x irradiation at LNT. It is normalized to its value for an x irradiation period of 100 min. The rate of formation of the Pb_2^{3+} dimers is fast at the beginning of the irradiation, but decreases after about 15 min. The fast for-

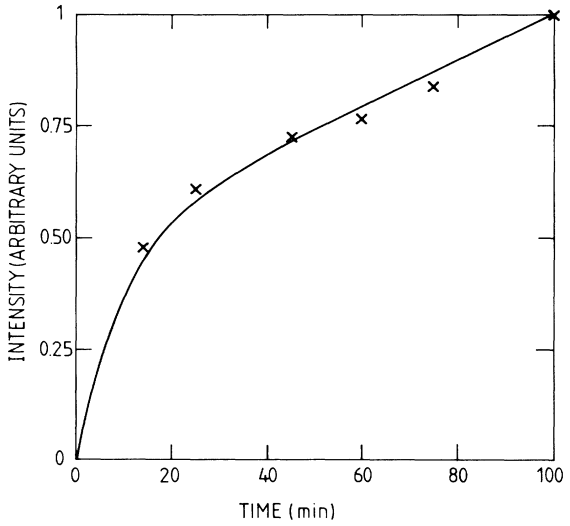

FIG. 5. The intensity of the Pb_2^{3+}(II) spectra is plotted as a function of the duration of x irradiation at LNT. It is normalized to its value after a period of 100 min of x irradiation.

mation during the first minutes of x irradiation would indicate that only simple processes such as hole or electron trapping are involved in the production of the centers. However, for such a production mechanism one usually finds a saturation in the concentration of the created defects. The relatively slow dropoff of the production rate, on the contrary, suggests the presence of additional time-consuming processes accompanying the hole and electron trapping. Since to our knowledge no interstitials or radiation-induced vacancies are involved in the Pb_2^{3+} defect structure, the retarding effect on the production of the center should possibly be sought in the formation of a dimer configuration of nearest-neighboring Pb^{2+} ions (see Sec. IV).

C. Pulse-anneal experiment after x irradiation at LNT

The temperature for maximal production of the Pb_2^{3+} defects is examined in a pulse-anneal experiment. A quenched NaCl:$PbCl_2$ crystal is x-irradiated for 2 h at LNT and subsequently annealed for 2 min at temperatures between LNT and RT. The intensity, plotted in Fig. 6 as a function of the annealing temperature, was measured (at $T=15$ K) as the mean value of the intensities of the different resonance lines belonging to the same defect. Nevertheless, we are dealing with a low accuracy on those results because of the overlap of resonance lines belonging to different centers.

Nevertheless, four stages can undoubtly be recognized in the annealing curves. The Pb_2^{3+}(I) and Pb_2^{3+}(II) spectra have a maximal intensity immediately after x irradiation. The intensity of the Pb_2^{3+}(I) spectrum for higher annealing temperatures decreases slowly and becomes undetectable at about 180 K, while the concentration of the Pb_2^{3+}(II) defect decreases much faster and disappears at about 150 K. Meanwhile the Pb_2^{3+}(III) defect is produced and reaches a maximal amount at 150 K. The decrease in concentration of the latter at about 210 K is correlated with the production of the Pb_2^{3+}(IV) defect with a maximum concentration at 240 K. This center disappears at 260 K and the Pb_2^{3+}(V) center is formed with maximum concentration at 280 K. As can be checked from Fig. 6, the temperature range in which each of the defects occur becomes smaller for higher production temperatures. At the same temperature stages some other minor defects were present. They seem to show the same characteristics as the Pb_2^{3+} defect; however, their intensity was too small to perform a quantitative analysis of their ESR spectra.

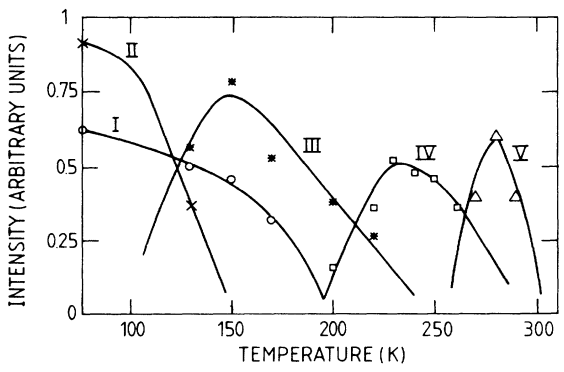

FIG. 6. The results of a pulse anneal experiment in which a NaCl:$PbCl_2$ crystal is x-irradiated during 90 min at LNT and subsequently annealed during 5 min at temperatures between 130 K and RT, are shown: ○, Pb_2^{3+}(I); ×, Pb_2^{3+}(II); *, Pb_2^{3+}(III); □, Pb_2^{3+}(IV); △, Pb_2^{3+}(V).

IV. DISCUSSION OF THE DEFECT STRUCTURE

As was already shown in the preceding sections, the essential core of all the centers, discussed in this paper, consists of an electron shared by two equivalent or nearly equivalent Pb^{2+} ions and, consequently, the nomenclature of Pb_2^{3+} centers was introduced. Since the Pb^{2+} ions are substitutional in two neighboring cation sites, the molecular axis is directed along a ⟨110⟩ crystallographic axis. First, this kind of model is strongly suggested by the observed hf structure. Second, the model is consistent with the symmetry of the resonance spectra. Finally, the identification of the different resonance lines with Pb_2^{3+} centers is supported by the production behavior of the centers under x irradiation and the need for quenching the crystal in order to disperse aggregates so as to obtain reasonable intensities of the centers.

Similar to the observation of many different "Pb^+(1)-type" centers in lead-doped KCl and RbCl, several Pb_2^{3+} centers, each showing the same essential features, are detected in NaCl:$PbCl_2$ crystals. In Refs. 13, 15, and 23-27 it was already suggested for divalent impurity ions like Pb^{2+}, Sn^{2+}, Mn^{2+}, and Fe^{2+} that small variations in the model of a given defect originate from different positions for the charge-compensating cation vacancy with respect to this ion. Corresponding to the production temperature and the symmetry of the centers various positions for this vacancy were proposed in order to construct a possible model, such as, e.g., for the Pb^+(1) defects in KCl and RbCl.[13]

The production temperature for each of the Pb_2^{3+} centers (Sec. III C) demonstrates that small modifications in the neighborhood of the essential Pb_2^{3+} structure occur as a result of higher annealing temperatures. It is still reasonable to attribute such changes in the crystal field experienced by the trapped electron dimer to displacements of the charge-compensating cation vacancies. But since, in principle, two cation vacancies are present in the environment of a lead dimer, many configurations can be constructed as possible models. This makes it impossible to suggest on the basis of the limited experimental results different models for each of the observed Pb_2^{3+} centers. Moreover, it is not excluded that the crystalline environment is changed locally by additional impurity ions such as oxygen. In the specific case of the oxygen impurity, however, its influence can be excluded, since no difference is observed in the resonance spectra of oxygen-free and oxygen-containing NaCl:$PbCl_2$ samples. Finally, it is possible that the local neighborhood of the dimer center is disturbed by the presence of a third IV dipole. Such a proposal can be suggested on the basis of the aggregation process, described in Ref. 9 as the growth of a trimer

from a mestastable dimer during the first stage of the clustering.

An interesting result is the absence of Pb_2^{3+} centers in KCl:$PbCl_2$ crystals. Samples with various lead concentrations have been x-irradiated at LNT either as-grown or after a storage period at RT. Such a handling still resulted in a small concentration of the $Pb^+(Cl_i^-)$ defect. This confirms again that the clustering proceeds faster in NaCl:$PbCl_2$ than in KCl:$PbCl_2$, in which almost no aggregation occurs during RT ageing.[11] On the other hand, an explanation for the lack of Pb_2^{3+} centers in KCl can be found in the different type of IV dipoles, present in the two alkali halides. In Ref. 6 the results of polarized luminescence experiments are explained as indicating that in KCl the charge-compensating cation vacancy is almost exclusively situated at a next-nearest-neighbor (NNN) position of the Pb^{2+} ion, while in the NaCl it is also located in a nearest-neighbor (NN) position of the Pb^{2+} ion. During x irradiation one of the Pb^{2+} ions of a dimer or even a trimer, constructed from NN IV dipoles, can easily capture an electron and subsequently jump to an adjacent cation vacancy in order to produce Pb_2^{3+} centers, as observed in NaCl [Fig. 7(a)]. Such a mechanism, however, is impossible from dimers or trimers, constructed from NNN IV dipoles, since two Pb^{2+} ions never can reach next-neighboring positions by only interchanging their position with a cation vacancy [Fig. 7(b)]. this difference was already formulated more generally in Ref. 9. There, it is suggested that mainly NN IV dipoles tend to form aggregates starting from a trimer to which dimers are added. In the last stage of the clustering process, they ultimately precipitate by a total rearrangement of the IV dipoles. The NNN dipoles, on the contrary, for dimers in which the impurity ions are separated by more than two lattice sites and these dimers directly precipitate to the Suzuki phase, already extensively examined in KCl:$PbCl_2$ crystals.[8] This behavior is also found in a theoretical calculation on the relative stability of various cluster configurations for different kinds of IV dipoles.[28] Unfortunately, this work does not include the results for lead-doped alkali halides, but the tendency, reported from experiments on those crystals, is in agreement with the results obtained for other divalent ions.

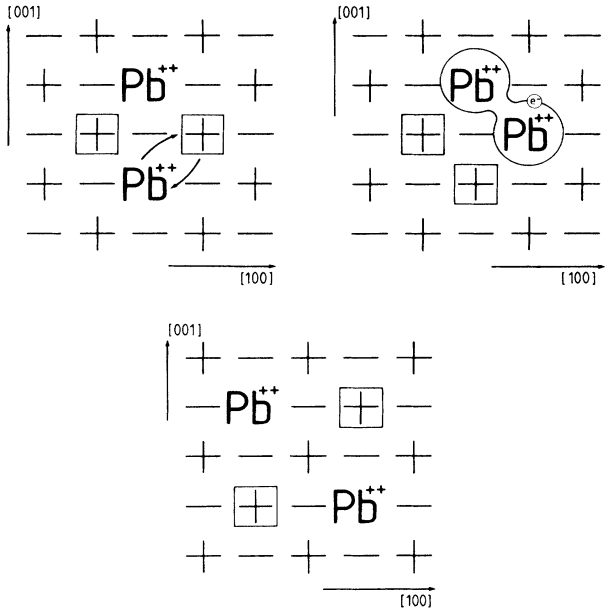

FIG. 7. In (a) the possible production mechanism for a Pb_2^{3+} center is given, starting from a dimer of nearest-neighbor IV dipoles, which occur in NaCl. In (b) a dimer of next-nearest-neighbor IV dipoles, occurring in KCl, is shown. Starting from such a situation no Pb_2^{3+}-center production is possible.

ACKNOWLEDGMENTS

We are indebted to Dr. S. V. Nistor for his advice in the initial experiments and to Dr. A. Bouwen for his experimental assistance. The IIKW (Interuniversitair voor Kernwetenschappen), the NFWO (National Fonds voor Wetenschappelijk Onderzoek), the Geconcerteerde Acties, and the PREST Program (Ministerie van Wetenschapsbeleid) are gratefully acknowledged for financing this work, as is the IWONL (Instituut voor Wetenschappelijk Onderzoek in Nijverheid en Landbouw) for financial support to one of the authors (I.H.).

[1]F. Agullo-Lopez, F. Cusso, C. Zaldo, J. Garcie Solé, F. Jaque, P. Aceituno, A. de Andrés, and J. M. Calleja, in *Induced Defects in Insulators,* edited by P. Mazzoldi (Les éditions de Physique, Paris, 1984), p. 117.

[2]J. S. Cook and J. S. Dryden, Proc. Phys. Soc. London **18**, 479 (1962).

[3]H. F. Symmons and R. C. Kemp, Brit. J. Appl. Phys. **17**, 607 (1966).

[4]F. Rodriquez and M. Moreno, Solid State Commun. **58**, 701 (1986).

[5]J. S. Dryden and G. G. Harvey, J. Phys. C **2**, 603 (1969).

[6]W. C. Collins and J. H. Crawford, Jr., Solid State Commun. **9**, 853 (1971).

[7]L. Marculescu, Phys. Status Solidi B **80**, 265 (1977).

[8]S. Bencie, R. Cappeletti, F. Fermi, M. Manfredi, J. Z. Damm, and E. Mugenski, J. Lumin. **18/19**, 341 (1979).

[9]J. E. Strutt and E. Lilley, Phys. Status Solidi A **33**, 229 (1976).

[10]A. I. Sors and E. Lilley, Phys. Status Solidi A **32**, 533 (1975).

[11]C. Zaldo, J. Garcia Solé, and F. Agullo-Lopez, J. Phys. Chem. Solids **43**, 837 (1982).

[12]E. Goovaerts, S. V. Nistor, and D. Schoemaker, Phys. Rev. B **28**, 3712 (1983).

[13]I. Heynderickx, E. Goovaerts, S. V. Nistor, and D. Schoemaker, Phys. Status Solidi B **136**, 69 (1986).

[14]D. Schoemaker and J. L. Kolopus, Solid State Commun. **8**, 435 (1970); W. Frey, R. Huss, H. Seidel, and E. Werkmann, Phys. Status Solidi B **68**, 257 (1975).

[15]E. Goovaerts, S. V. Nistor, and D. Schoemaker, Phys. Rev. B **25**, 83 (1982).

[16]J. P. Stott and J. H. Crawford, Phys. Rev. B **4**, 639 (1971).

[17]B.-R. Yang, E. Goovaerts, and D. Schoemaker, Phys. Rev. B **27**, 1507 (1983).
[18]S. V. Nistor, E. Goovaerts, B.-R. Yang, and D. Schoemaker, Phys. Rev. B **28**, 1219 (1983).
[19]D. Schoemaker, Phys. Rev. B **7**, 786 (1973).
[20]I. Heynderickx, H. De Raedt, and D. Schoemaker, J. Magn. Reson. **70**, 134 (1986).
[21]A. Abragam and B. Bleaney, *Electron Paramagnetic Resonance of Transition Ions* (Clarendon, Oxford, 1970).
[22]I. Heynderickx, E. Goovaerts, and D. Schoemaker, Solid State Commun. **55**, 877 (1985).
[23]C. J. Delbecq, R. Hartford, D. Schoemaker, and P. H. Yuster, Phys. Rev. B **13**, 3631 (1976).
[24]D. Schoemaker, I. Heynderickx, and E. Goovaerts, Phys. Rev. B **31**, 5687 (1985).
[25]G. Watkins, Phys. Rev. **113**, 79 (1959).
[26]B.-R. Yang, A. Bouwen, and D. Schoemaker, Phys. Status Solidi B **127**, 657 (1985); S. V. Nistor, M. Velter-Stefănescu, and C. D. Matescu, Solid State Commun. **53**, 989 (1985).
[27]F. Van Steen and D. Schoemaker, Phys. Rev. B **19**, 55 (1979).
[28]J. Corish and J. M. Quigley, in *Computer Simulation of Solids,* edited by C. R. A. Catlow and W. C. Mackerödt (Springer-Verlag, New York, 1982), Chap. 17.